Atmos. Chem. Phys., 12, 3821–3835, 2012
www.atmos-chem-phys.net/12/3821/2012/
doi:10.5194/acp-12-3821-2012

Atmospheric Chemistry and Physics

Unusually low ozone, HCl, and HNO_3 column measurements at Eureka, Canada during winter/spring 2011

R. Lindenmaier[1,*], K. Strong[1], R. L. Batchelor[2], M. P. Chipperfield[3], W. H. Daffer[4], J. R. Drummond[5], T. J. Duck[5], H. Fast[6], W. Feng[3,7], P. F. Fogal[1,6], F. Kolonjari[1], G. L. Manney[4,8], A. Manson[9], C. Meek[9], R. L. Mittermeier[6], G. J. Nott[5], C. Perro[5], and K. A. Walker[1]

[1]Department of Physics, University of Toronto, 60 St. George Street, Toronto, Ontario, M5S 1A7, Canada
[2]Atmospheric Chemistry Division, National Center for Atmospheric Research, 3450 Mitchell Lane, Boulder, Colorado, 80310, USA
[3]Institute for Climate and Atmospheric Science, School of Earth and Environment, University of Leeds, Leeds, LS2 9JT, UK
[4]Jet Propulsion Laboratory, California Institute of Technology, 4800 Oak Grove Drive, Pasadena, California, 91109, USA
[5]Department of Physics and Atmospheric Science, Dalhousie University, 6310 Coburg Road, Halifax, Nova Scotia, B3H 1Z9, Canada
[6]Air Quality Research Division, Environment Canada, 4905 Dufferin St., Toronto, Ontario, M3H 5T4, Canada
[7]National Centre for Atmospheric Science, School of Earth and Environment, University of Leeds, Leeds, LS2 9JT, UK
[8]Department of Physics, New Mexico Institute of Mining and Technology, Socorro, New Mexico, 87801, USA
[9]Institute of Space and Atmospheric Studies, University of Saskatchewan, Saskatoon, Saskatchewan, S7N 5E2, Canada
[*]now at: Los Alamos National Laboratory, Los Alamos, 87545, USA

Correspondence to: R. Lindenmaier (rodica@atmosp.physics.utoronto.ca)

Received: 3 October 2011 – Published in Atmos. Chem. Phys. Discuss.: 11 January 2012
Revised: 6 April 2012 – Accepted: 10 April 2012 – Published: 27 April 2012

Abstract. As a consequence of dynamically variable meteorological conditions, springtime Arctic ozone levels exhibit significant interannual variability in the lower stratosphere. In winter 2011, the polar vortex was strong and cold for an unusually long time. Our research site, located at Eureka, Nunavut, Canada (80.05° N, 86.42° W), was mostly inside the vortex from October 2010 until late March 2011. The Bruker 125HR Fourier transform infrared spectrometer installed at the Polar Environment Atmospheric Research Laboratory at Eureka acquired measurements from 23 February to 6 April during the 2011 Canadian Arctic Atmospheric Chemistry Experiment Validation Campaign. These measurements showed unusually low ozone, HCl, and HNO_3 total columns compared to the previous 14 yr. To remove dynamical effects, we normalized these total columns by the HF total column. The normalized values of the ozone, HCl, and HNO_3 total columns were smaller than those from previous years, and confirmed the occurrence of chlorine activation and chemical ozone depletion. To quantify the chemical ozone loss, a three-dimensional chemical transport model, SLIMCAT, and the passive subtraction method were used. The chemical ozone depletion was calculated as the mean percentage difference between the measured ozone and the SLIMCAT passive ozone, and was found to be 35 %.

1 Introduction

Significant springtime polar stratospheric ozone depletion was first observed at the British Antarctic Survey station at Halley Bay (Farman et al., 1985). It was later shown that the large ozone loss over Antarctica in late winter is caused by chlorine chemistry in the presence of polar stratospheric clouds (PSCs) (Solomon et al., 1986). Although not as large as the chemical ozone depletion observed in Antarctica, Arctic lower stratospheric ozone can also be destroyed by similar processes. During the polar winter, heterogeneous reactions on the surfaces of stratospheric particles at cold temperatures convert the chlorine reservoir species HCl and $ClONO_2$ to active chlorine, which participates in springtime

ozone destruction (Solomon et al., 1986). The background stratospheric aerosols formed by liquid-phase binary sulfuric acid/water (H_2SO_4/H_2O) droplets are found globally throughout the stratosphere. Inside the vortex, where temperatures are very low, these take up nitric acid (HNO_3) and H_2O (Carslaw et al., 1994; Tabazadeh et al., 1994) transforming into ternary $HNO_3/H_2SO_4/H_2O$ droplets, usually referred to as supercooled ternary solution (STS) PSCs that further freeze to nitric acid trihydrate (NAT). H_2O ice and solid hydrates of HNO_3 are other forms for PSC particles (Voigt et al., 2000).

Based on their optical parameters, PSCs are classified as type I, which usually form at temperatures of ∼195 K (the NAT equilibrium temperature for typical partial pressures of water vapor and HNO_3 in the lower stratosphere), and type II, which form at temperatures lower than the stratospheric ice frost point of ∼188 K (Steele et al., 1983). During the polar winter, a mixture of liquid binary or ternary droplets and solid particles, NAT, and H_2O, of various sizes and number densities can be found in the stratosphere (Toon et al., 2000; Drdla et al., 2003). It has been shown that chlorine activation rates on stratospheric particles depend on the uptake coefficient of the particle and the particulate surface area density (Lowe and MacKenzie, 2008). These are generally much larger for the STS compared to the NAT PSC particles, making liquid particles much more efficient in chlorine activation (Portmann et al., 1996; Lowe and MacKenzie, 2008). In the Arctic, the STS PSCs are common, but the temperature distribution and the volume of air in which the PSCs can exist depend very much on the dynamical situation of each winter (Pawson and Naujokat, 1999). As a consequence, chemical ozone loss in the Arctic vortex can vary considerably from year to year depending on the stratospheric meteorology (e.g., Manney et al., 2003; Rex et al., 2004; Goutail et al., 2005; Feng et al, 2007).

The Northern Hemisphere winter polar vortex typically forms in the lower stratosphere early in November, is strongest in mid-January and dissipates in late March or early April (WMO, 2011). Its dynamical variability changes from year-to-year and as such, quantifying Arctic ozone loss is difficult since it requires the effects of chemical processes to be distinguished from those of transport and mixing (Tegtmeier et al., 2008). The period between 1989/1990 and 1997/1998 was characterized by reduced dynamical variability, with nine consecutive years without a major stratospheric warming (Pawson et al., 1998; Labitzke et al., 2002).

The polar vortex that formed in the 1996/1997 winter-spring persisted in the lower stratosphere into May (Manney et al., 1997). Temperatures below the 195 K PSC threshold persisted into late March, leading to a column ozone loss of 10 % due to chemical depletion for the period from late January to early April 1997 (Donovan et al., 1997; Fioletov et al., 1997; Manney et al., 1997; Newman et al., 1997). A larger proportion of column ozone anomaly, however, arose from dynamical effects, from the unusually prolonged cold period (e.g., Petzoldt, 1999) and from underlying tropospheric disturbances (e.g., Orsolini et al., 1998).

Since 1998/1999, there have been several warmer-than-average and dynamically disturbed winters: 1998/1999, 2000/2001, 2001/2002, 2003/2004, 2005/2006, 2008/2009, and 2009/2010 (WMO, 2007; WMO, 2011), combined with cold winters in 1999/2000 (Mellqvist et al., 2002; Müller et al., 2003), 2002/2003 (WMO, 2007), 2004/2005 (Jin et al., 2006; Rösevall et al., 2008), 2006/2007 (Rösevall et al., 2007), and 2007/2008 (WMO, 2011). These cold winters were characterized by chemical ozone depletion, with reported reductions in the ozone column ranging from 80 to 135 DU.

In winter 2010/2011, another cold and strong Arctic vortex formed (Manney et al., 2011). It was located above our research site, Eureka, for much of the time until late March. This paper reports unusually low ozone, HCl, and HNO_3 column measurements at Eureka, compared to measurements from previous years. The measurements were made with the Bruker 125HR Fourier transform infrared (FTIR) spectrometer during the 2011 Canadian Arctic Atmospheric Chemistry Experiment (ACE) Validation Campaign, which took place from 21 February to 6 April.

The paper is organized as follows: Sect. 2 introduces the measurement site and the instruments. Section 3 presents the meteorological conditions during the winter-spring 2010/2011, describes our measurements, and compares them with results from the previous 14 yr. The chemical ozone loss is quantified in Sect. 4, followed by a summary of the results in Sect. 5.

2 Measurements

2.1 CANDAC Bruker IFS 125HR

The Polar Environment Atmospheric Research Laboratory (PEARL) was established in 2005 by the Canadian Network for the Detection of Atmospheric Change (CANDAC) in the Canadian high Arctic. It is located on Ellesmere Island at Eureka, Nunavut (80.05° N, 86.42° W) at 610 m above sea level. The high-resolution Bruker 125HR FTIR spectrometer (henceforth called the 125HR) was installed in July 2006 at PEARL and records solar absorption spectra throughout the sunlit part of the year (mid-February to mid-October) in the mid-infrared spectral range (600–4300 cm^{-1}). A comprehensive description of the instrument is given by Batchelor et al. (2009). Altitude-dependent volume mixing ratio (VMR) profiles were retrieved from the acquired spectra using SFIT2 (Pougatchev et al., 1995), a profile retrieval algorithm that employs the Optimal Estimation Method (OEM) developed by Rodgers (2000). The OEM is a regularization method that retrieves VMR profiles from a statistical weighting of the a priori information and the measurements. These profiles were converted to density profiles using temperature

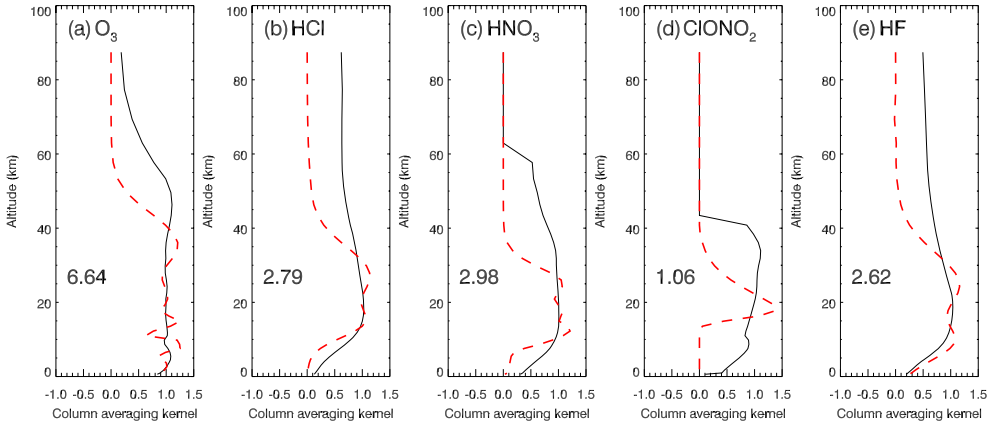

Fig. 1. Typical column averaging kernels (black solid line) and sensitivities (red dashed line) for the 125HR springtime measurements (calculated for 6 March 2009 at a solar zenith angle of 85.58°).

and pressure profiles and integrated throughout the column to yield the column densities. SFIT2 v.3.92c and the HITRAN 2004 + updates line list (Rothman et al., 2005) were used for the retrievals with the spectral microwindows, a priori profiles, and covariance matrices as described by Batchelor et al. (2009).

The averaging kernel matrix produced during the retrieval can be used to characterize the information content of the retrievals. Figure 1 shows typical column averaging kernels for the 125HR, along with the sensitivity (the sum of the elements of the averaging kernels) and the degrees of freedom for signal (DOFS), defined as the trace of the averaging kernel matrix. The sensitivity indicates the fraction of the retrieval at each altitude that comes from the measurement rather than the a priori (Vigouroux et al., 2008). The retrieval for each gas has good sensitivity in the lower stratosphere, with DOFS varying from 1.06 for $ClONO_2$ to 6.64 for ozone. Total columns from 0.61 to 100 km were calculated and used in this work.

The error calculations in this work are based on the methodology of Rodgers (1976, 1990), and the results are given in Table 1. In addition to smoothing error and measurement error, forward model parameter errors have been calculated as described by Rodgers (2000) using a perturbation method and our best estimate of the uncertainties in temperature, line intensity, air-broadened half width, and solar zenith angle. Interference errors, as described by Rodgers and Connor (2003) have been calculated to account for uncertainties in retrieval parameters (i.e., wavelength shift, instrument line shape, background slope and curvature, and phase error) and in the interfering gases simultaneously retrieved. The total error was calculated by adding all these errors in quadrature. The error budget calculation is described by Batchelor et al. (2009).

Table 1. Springtime mean (for the period 24 February to 6 April) total errors for ozone, HCl, HNO_3, $ClONO_2$, and HF total columns retrieved from the FTIR spectra. The total error was calculated as described in Sects. 2.1 and 2.2, respectively.

	Total error (%)	
	125HR	DA8
O_3	4.5	11.3
HCl	3.7	12.3
HNO_3	13.5	16.9
$ClONO_2$	4.5	18.2
HF	4.7	13.2

2.2 Environment Canada ABB Bomem DA8

The Environment Canada ABB Bomem DA8 FTIR spectrometer (henceforth the DA8) was installed at Eureka in 1993 and acquired solar absorption spectra each spring through to 2008 (Donovan et al., 1997; Farahani et al., 2007; Paton-Walsh et al., 2008; Fast et al., 2011; Fu et al., 2011). An intercomparison of the DA8 and 125HR measurements was conducted by Batchelor et al. (2010). The DA8 spectrometer is a vertically aligned Michelson interferometer that, similarly to the 125HR, records high-resolution solar absorption spectra over the spectral range from 700 to 5000 cm^{-1}. The spectra were analyzed using the SFIT1 spectral fitting routine (Rinsland et al., 1982, 1988), using the line parameters in the HITRAN 1992 compilation (Rothman et al., 1992) plus updates. Scaling factors derived from the fits were applied to the a priori VMR profiles at all altitude layers to obtain the final scaled profiles. These profiles were combined with the density-weighted pressure and temperature profiles to generate the column profiles, which were integrated to derive the column densities. In this work, these DA8 total columns were scaled prior to comparison with the 125HR total columns to account for the bias induced by the

use of a different retrieval algorithm and line list. The biases in the DA8 measurements relative to those retrieved with the HITRAN 2004 compilation and SFIT2 are −3.9 % for ozone, −0.4 % for HCl, −14.3 % for HNO_3, +15.6 % for $ClONO_2$, and 0.0 % for HF as shown by Fast et al. (2011). The same paper also describes the error budget calculation for the errors presented in Table 1. The total error was calculated considering the instrumental error, errors arising from the retrieval algorithm and from the chosen microwindow, uncertainties introduced by the a priori VMR profile, uncertainties due to temperature and solar zenith angle, spectral signal-to-noise ratio and spectral fitting. In this paper, we present DA8 results for 10 yr from 1997 to 2006, to provide a 15-year record for the trace gas comparisons.

2.3 CANDAC Rayleigh-Mie-Raman Lidar

The CANDAC Rayleigh-Mie-Raman Lidar (CRL) is a ground-based lidar system installed at the Zero Altitude PEARL Auxiliary Laboratory (ØPAL) at Eureka. The CRL transmits at 532 nm and 355 nm using two Nd:YAG lasers with repetition rates of 10 Hz. The CRL has eight detection channels: vibrational and pure-rotational Raman channels for the measurement of tropospheric molecular nitrogen, water vapor and temperature profiles, along with two elastic backscatter channels. The 532 nm and 355 nm elastic channels can be used for PSC detection and for characterization and determination of aerosol/cloud backscatter ratio. The depolarization ratio can also be calculated at 532 nm allowing for the discrimination between liquid and solid phase cloud particles. For a complete description of the instrument see Nott et al. (2011).

2.4 Radiosondes

Balloon-borne radiosondes measure profiles of atmospheric temperature, pressure and humidity. Radiosonde observations are taken year round at Eureka twice daily, at 6 a.m. and 6 p.m. (corresponding to 11 a.m. and 11 p.m. Universal Time) using Vaisala RS92 radiosondes. These have an accuracy of ±0.5 hPa for pressure, ±0.5 K for temperature, and ±3.5 % for relative humidity (Vömel et al., 2007; Steinbrecht et al., 2008). The data from the balloon are transmitted continuously to the launching station, where they are interpreted and entered into Environment Canada's Upper Air Archive.

3 Results and discussion

3.1 Arctic meteorological conditions

The polar vortex dominates the winter dynamics of the stratosphere and has a profound effect on the distribution of chemical constituents. Before analyzing the evolution of the trace gas columns above Eureka, it is useful to know what the Arctic meteorological conditions were during the 2010/2011 winter-spring. Since the Northern Hemisphere polar vortex can be highly variable on both horizontal and vertical spatial scales throughout its life cycle, it is important to determine the vortex edge evolution on multiple heights in the atmosphere, which contribute significantly to the 125HR column measurements. The vortex edge was determined using the Q-diagnostic and the algorithm developed by Harvey et al. (2002), which has been used in other studies to characterize the polar vortex (Chshyolkova et al., 2007; Manson et al., 2008; Xu et al., 2009). The scalar quantity Q is a measure of the relative contribution of strain and rotation in the wind field, derived from the Met Office (MetO) analyses (Swinbank and O'Neill, 1994). To identify the vortex edge, Q was integrated along the stream function contours. A detailed description of the Q-diagnostic method can be found in Fairlie (1995) and Harvey et al. (2002) and references therein. For the Eureka measurements discussed in Sect. 3.3, the temporal evolution of scaled potential vorticity is shown. Vortex edge identification using a scaled PV (sPV, PV scaled so as to have a similar range of values at levels throughout the stratosphere) contour was used by Manney et al. (2007). This method is most robust in the lower and middle stratosphere when the vortex is strong and well defined, as was the case during winter/spring 2011. Results using sPV to identify the vortex edge agree closely with those using the PV gradient × windspeed criterion and other criteria (e.g., that of Nash et al., 1996 and the Q-diagnostic), based on PV gradients (Manney et al., 2007).

A movie showing the evolution of the vortex in the Northern Hemisphere can be found at http://www.usask.ca/physics/isas/vtex11jfm.gif, and is included as Supplement. It shows that on day 37 (6 February), the vortex moved above Eureka and stayed above our site until day 83 (24 March). In Fig. 2, the edge of the vortex on the 525-K isentropic surface (∼21 km altitude) is indicated, along with the temperatures on the same level. The first panel corresponds to day 54 (23 February), the first day of the 125HR measurements. The following panels have a 5-day time step, and the last panel corresponds to day 96 (6 April), the last day of the campaign. A second movie showing the evolution of the temperatures can be found at http://www.usask.ca/physics/isas/tk10-11.gif, and is also included as supplementary material.

The minimum temperatures inside the vortex during winter/spring 2010/2011 were persistently cold, staying below the PSC formation threshold for more than 100 days (Manney et al., 2011). On the 525-K level, temperatures within the vortex first dropped below the type I PSC threshold (195 K) on day 330 of 2010 (27 November) and continued to decrease (as shown in the movie). They dropped below 190 K (the precision is limited by the temperature step of 5 K in the plots) on day 353 (20 December), remaining low until 11 January. On day 21 in 2011 (21 January), the temperatures again fell below 190 K until day 60 (1 March) except on days 17, 18, and 31–35 (17, 18 and 31 January–4 February). The temperatures continued to oscillate between 190 and 195 K from

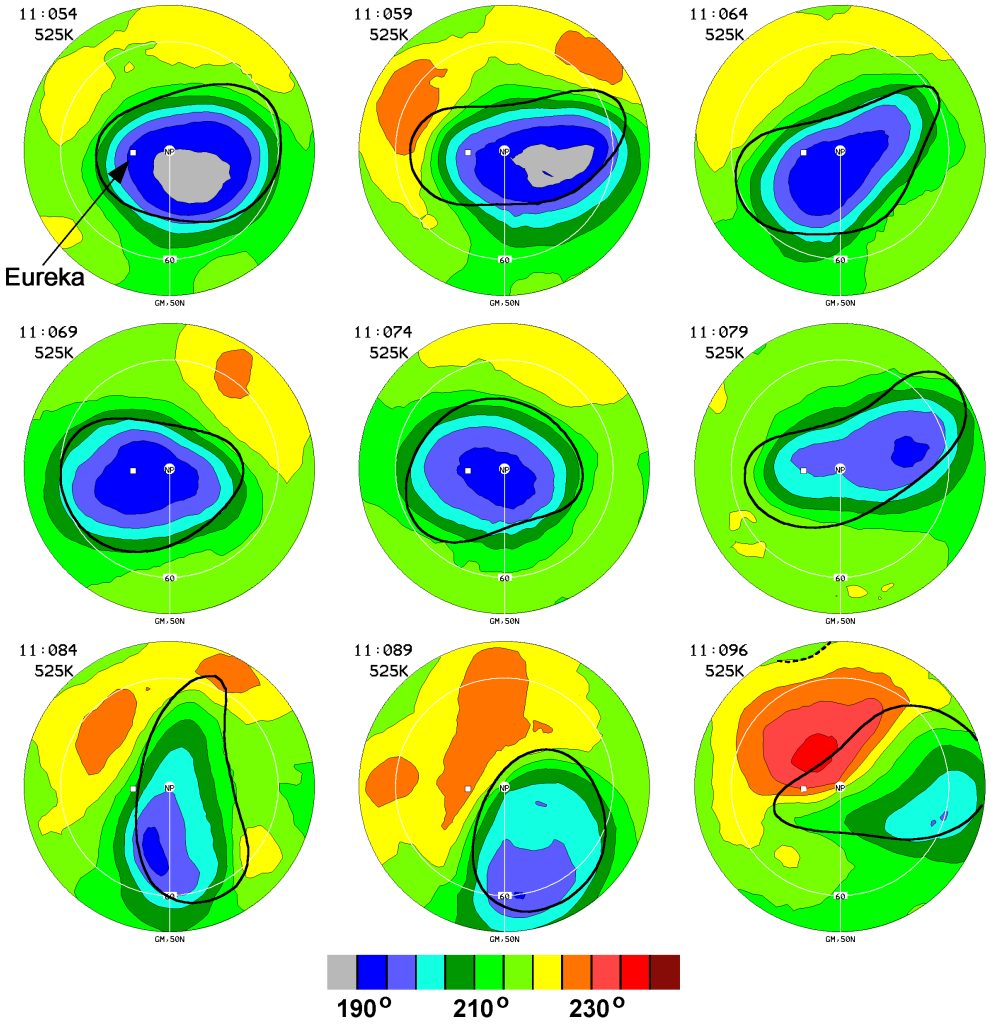

Fig. 2. MetO 5-K temperature contours for the 525-K potential temperature level (color-coded as shown in the legend), with the overlaid vortex edge for the same level (black solid line). These contours correspond to the days shown on the top left side of each map. The white square indicates the location of Eureka, while the white circle indicates 60° N latitude. The southern boundary is at 50° N.

day 60 (1 March) to day 90 (31 March), when they increased above 195 K, and remained above this threshold for the remainder of the spring (Manney et al., 2011).

3.2 Temperature measurements and PSC observations at Eureka

The Eureka radiosonde temperature profiles, presented in Fig. 3, show the evolution of temperature at each altitude during February (top panels) and March (bottom panels). For each month, these are split into three periods for clarity. The type I and II PSC threshold temperatures are also shown. From 7 February to the end of the month, the temperatures dropped below the type I PSC threshold at altitudes of ∼17 to 24 km, reaching the type II PSC threshold from 20 to 23 km on 14 and 15 February. NASA's Cloud-Aerosol Lidar and Infrared Pathfinder Satellite Observation (CALIPSO) showed the presence of PSCs near Eureka between 11 and 17 February between 18 and 23 km (not shown, images can be found at: http://www-calipso.larc.nasa.gov/products/lidar/browse_images/show_calendar.php.

The CRL was not operational at that time (it started operation on 20 February), but indicated the presence of PSCs above Eureka during March (Fig. 4). The backscatter ratios at 532 nm for 8–12 March show that the cloud has two dominant layers centered at 15 and 18 km. The mean backscatter ratio of the background aerosol at 11-13 km, where the temperatures were greater than 200 K, was 1.13±0.1. This was taken as the background aerosol backscatter ratio for comparison with the clouds, whose backscatter ratio varied between 1.3 and 2.3. The clouds had a depolarization ratio of approximately 10 % and this, along with the enhanced backscatter ratio, indicates mixed-phase type I PSCs (Pitts et al., 2009) during this period. As can be seen in Fig. 3, the temperatures

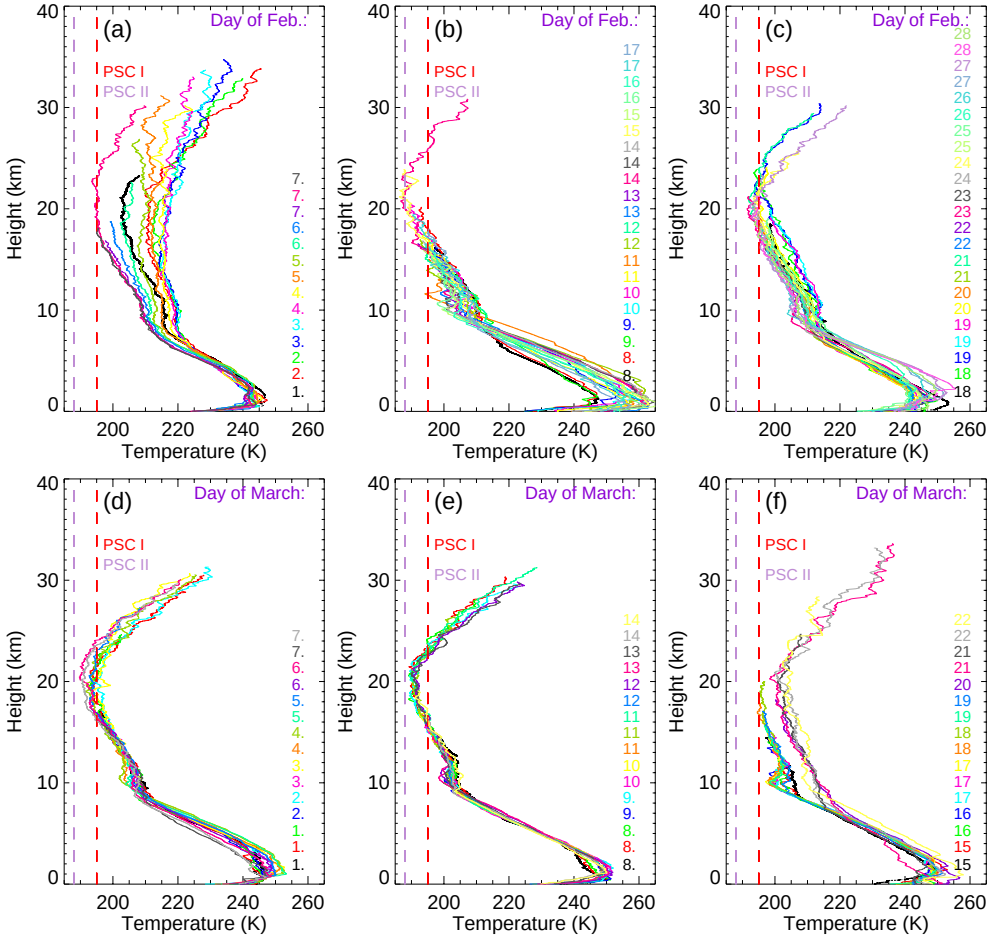

Fig. 3. Radiosonde temperature profiles for 1 to 28 February (panels **a–c**) and 1 to 22 March (panels **d–f**). The day is shown on the right side of each panel, color coded. The two dashed vertical lines correspond to the threshold temperature values for the formation of PSC type I (red) and PSC type II (purple). The division of days per plot was chosen to make the temperature drop below the PSC type I or PSC type II thresholds more visible.

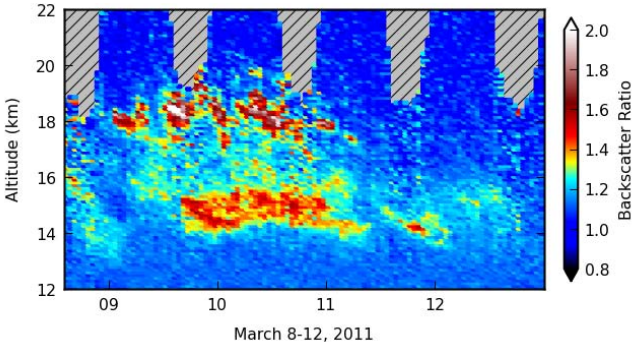

Fig. 4. Backscatter ratio at 532 nm as measured by the CRL for 8 to 12 March. The hashed areas represent data that were considered to be noise.

from 15 to 24 km during this period were below the threshold for type I PSC formation but above that for type II clouds. PSCs were observed by the CRL as late as 18 March (not shown), much later into the season than PSCs are usually seen in the Arctic (Langematz and Kunze, 2006).

3.3 Total column measurements

In 2011, the 125HR began acquiring useful data on 24 February (at solar zenith angles, SZA, between 89° and 90°) and results are reported here through 6 April (at SZA between 73° and 78°), the end of an intensive period of measurements that were made as part of the Canadian Arctic ACE Validation Campaign. There are some gaps in the data, particularly in late March, due to cloudy and unsettled weather. From these measurements, ozone, HCl, HF, HNO_3, and $ClONO_2$ vertical profiles were retrieved, and total columns were calculated. The results are discussed and compared with total columns from previous years. Note that we neglected species trends in our comparisons, as they are very small compared to the changes of dynamical or chemical origin (e.g., see

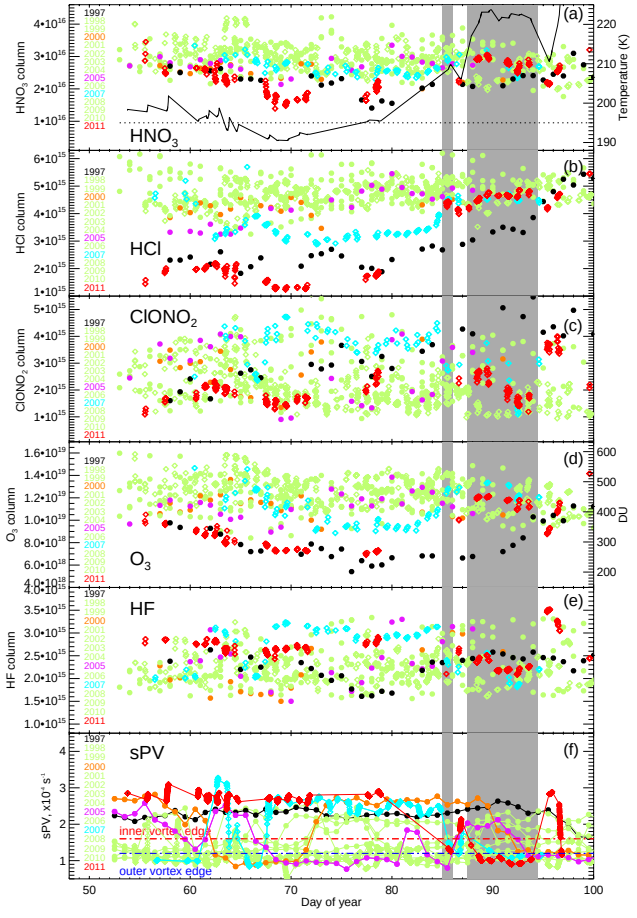

Fig. 5. From **(a)** to **(e)**, spring time series of HNO_3, HCl, $ClONO_2$, ozone, and HF total columns from 1997 to 2011, respectively. Filled circles represent DA8 measurements and open diamonds represent 125HR measurements. The colors correspond to different years as shown in the legend. For ozone, panel **(d)**, the left y-axis gives the column amounts in molec cm^{-2}, while the right y-axis gives the column amounts in Dobson units (DU). Panel **(a)** also shows the evolution of the temperature at 21 km along the 125HR line-of-sight for the measurements at Eureka (black solid line) and the threshold temperature value for the formation of type I PSCs (black dotted line). Panel **(f)** shows the evolution of sPV at 21 km above Eureka (as described in the text), for all years as shown in the legend. For the years with 125HR data, sPV is only shown for days when measurements were made. The red and blue dot-dash lines show the inner (red) and the outer (blue) vortex edge, respectively. The gray shading highlights the days when the instrument sampled air masses on the edge or outside the vortex.

Vigouroux et al., 2002; SPARC CCMVal, 2010; Kohlhepp et al., 2012).

Figure 5 shows total columns of the gases mentioned above, along with the evolution of the scaled potential vorticity at Eureka for each year. For 1997–2006 (years with daily average DA8 measurements), sPV was calculated daily at 12:00 UT using MERRA (Modern Era Retrospective-analysis for Research and Applications) analyses (Rienecker et al., 2011) for the 21-km altitude above Eureka. For 2007–2011 (years with 125HR measurements), sPV was calculated at 21 km along the 125HR line-of-sight using the GEOS version 5.2.0 (GEOS-5) analyses (Rienecker et al., 2008) and is only shown for days with 125HR measurements. An sPV of 1.2×10^{-4} s^{-1} was used as proxy for the outer edge of the polar vortex and sPV of 1.6×10^{-4} s^{-1} was used for the inner edge (Manney et al., 2007). While during some years, the instruments sampled mostly inside the polar vortex (e.g., 1997, 2000, 2004, 2005, 2007, 2011), for other years they measured mostly outside the vortex (e.g., 1999, 2001, 2008, 2009, 2010).

In 2011, our sampled air masses were well inside the vortex from the start of the measurements until day 78 (19 March). For the remainder of the campaign, the 125HR sampled through the edge of the vortex or outside, except on day 86 (27 March) and days 95 and 96 (5 and 6 April). The gray shading highlights the days in 2011 when the instrument sampled air masses on the edge or outside the vortex. Note that the daily sequence of MetO images that shows the vortex edge (Q-diagnostic) for days 50 to 100 on the 525-K surface (Fig. 2) agrees very well with the combination of GEOS-5/sPV used in the remainder of the analyses shown in this paper. For days 53 to 84 and 88 to 93, both vortex-edge methods agree in showing Eureka inside and outside the vortex, respectively. The only mild disagreement occurs on day 87, when the combination of GEOS-5 with sPV contours indicated Eureka inside the vortex or on the edge depending upon the height, while both GEOS-5 and MetO using the Q-diagnostic at 525 K (∼21 km) showed Eureka on the edge.

The 2011 gas-phase HNO_3 total columns, Fig. 5a red diamonds, decrease slowly until day 64 (5 March), followed by a sharp decrease with a minimum on day 68 (9 March) and low values until day 77 (18 March). The instrument sampled air inside the vortex through all these days. The solid black line represents the temperature along the 125HR line-of-sight at 21 km. The minimum HNO_3 column occurs at the time when the temperature was well below the type I PSC temperature threshold, indicating that HNO_3 had been taken up onto the surfaces of (liquid or solid) PSC particles. The minimum HNO_3 total column is 1.39×10^{16} molec cm^{-2}, approximately the same as the 1997 (black circles) minimum seen on day 78 (19 March). The minima measured during these two years stand out from the HNO_3 total column values measured during the past 15 yr. 2000, 2005 and 2007 are also highlighted, as these three years were cold and characterized by chemical ozone depletion (Jin et al., 2006; Manney et al., 2006; Rex et al., 2006; Rösevall et al., 2007; Singleton et al., 2007; WMO, 2007; Rösevall et al., 2008; WMO, 2011).

The evolution of the chlorine reservoir HCl is shown in Fig. 5b. The 2011 total columns are persistently lower than all previous years for days 55–78 (24 February–19 March). The 2011 HCl total columns reached a minimum of $\sim1.2\times10^{15}$ molec cm^{-2} on days 68–71 (9–12 March), indicating chlorine activation, and then gradually increased.

Beginning on day 77, the chlorine slowly converted back into its HCl reservoir, as shown by the recovery of HCl inside the vortex. This recovery continued until the last day of measurements. For comparison, in 1997 the maximum reduction in HCl occurred on day 64 (5 March). For the other years, no extreme values were observed, although low values can be seen for days 58 (27 February) to 65 (6 March) and 68 (9 March) to 83 (24 March) in 2005 and 2007, respectively.

Total columns of the second chlorine reservoir, $ClONO_2$, are shown in Fig. 5c. The minima seen for 2005 correspond to measurements outside the vortex, as shown in panel 5f. The 2011 values are in the lower range of columns measured over the past 15 yr. At the beginning of the 2011 campaign, the $ClONO_2$ total columns are close to the values measured in 1997. After day 59 (28 February), the 1997 total columns increase, while the 2011 ones remain low, increasing on day 77 (18 March). Note that during days 68–71, there is a small decrease in the $ClONO_2$ column, which coincides with the HCl decrease and suggests that chlorine activation is occurring. The increase on day 77 that persisted inside the vortex until the end of the campaign shows the conversion of active chlorine to its $ClONO_2$ reservoir. When PSCs can no longer form and the active chlorine reverts to its reservoir species, the resulting repartitioning of the chlorine in the Arctic typically results in enhanced $ClONO_2$ and sustained low values of HCl for some time after PSCs have disappeared (Santee et al., 2008). The enhancement in $ClONO_2$ is due to the reaction of NO_2 with ClO, which is more rapid than the competing reaction of active chlorine to form HCl, and is followed by a slow repartitioning between $ClONO_2$ and HCl over the following weeks. However, in 2011, the conversion of active chlorine back into these two reservoirs was simultaneous, differing from the usual repartitioning. This suggests that the NO_2 necessary for $ClONO_2$ to form was less abundant than in previous years, possibly due to permanent removal through PSC sedimentation (Manney et al., 2011).

Figure 5d shows the evolution of ozone total columns. The columns slowly decrease, with the lowest ozone column seen on day 77, being 6.9×10^{18} molec cm^{-2} (257 DU). This minimum follows after the chlorine activation and is consistent with chemical ozone destruction. However, the unusually persistent cold in 2011 would have resulted in lower column ozone than in most previous Arctic winters even in the absence of chemical loss (Petzoldt, 1999; Manney et al., 2011). The evolution of column ozone in 1997 was dominated by dynamical effects (Petzoldt, 1999) and the chemical ozone depletion was modest in that year. The 1997 ozone total columns slowly decrease in the first half of the interval, followed by the ozone minimum on day 76 (17 March) and then by a gradual recovery. For 1997, the minimum value was 5.4×10^{18} molec cm^{-2} (201 DU). Low ozone was also seen in 2007, when the 125HR sampled inside the vortex for approximately two weeks (as shown in Fig. 5f), but those total columns are $\sim$100 DU larger than the 2011 total columns. For the other years, both day-to-day and interannual variability are observed (being in agreement with the evolution of the vortex above Eureka shown in Fig. 5f for each year), but none of the minima are as pronounced as those in 1997 and 2011.

HF is a long-lived tracer of vertical motion in the stratosphere (Mankin et al., 1990; Toon et al., 1992). It is produced in the stratosphere through photodissociation and is chemically unreactive. If an air column is displaced downward, with replacement at the top by air from neighboring columns, then the total column abundance of HF will increase. Since the temperatures inside the vortex were low, we expect the cold air to sink and for all air masses sampled inside the vortex, the HF total columns to be larger than those outside the vortex. During 2011, HF total columns (Fig. 5e) are large and relatively constant through days 55–83 (24 February–24 March) when the instrument sampled air masses inside the vortex, decreasing and then increasing after day 84 (25 March) as the instrument sampled air outside and then inside the vortex, respectively.

3.4 Normalizing with HF

Because dynamical effects usually dominate the evolution of the column ozone in the Arctic, in order to assess the degree to which changes in the total columns of ozone, HCl, HNO_3, and $ClONO_2$ are due to chemical processing, we normalized the measured total columns of these species with the HF columns. HF is a good dynamic tracer; the VMR profiles of ozone, HCl, HNO_3, and $ClONO_2$ generally correlate well with the HF profile in the lower stratosphere, where most of their column abundances reside, so that vertical transport will change their vertical column abundances proportionally (Toon et al., 1999). Another important advantage is that there is very little tropospheric contribution to the HF total column, which could otherwise mask variations due to stratospheric transport. Thus, the normalization with HF removes many dynamical effects, such as diabatic descent and tropopause height changes (Toon et al., 1999; Mellqvist et al., 2002).

Figure 6 shows the normalized total columns of HNO_3, HCl, $ClONO_2$, and ozone. The shaded area highlights the days of 2011 when the instrument sampled the air on the edge or outside the vortex (as in Fig. 5). We assume that if the normalized value for any of these gases decreases inside the vortex, this is due mainly to chemical processes.

For 2011, the HNO_3/HF ratios (Fig. 6a) have the same evolution as the HNO_3 total columns in Fig. 5a. The slow decrease in the normalized HNO_3 values from the beginning of the measurements to day 64, followed by the sharp decrease on day 68, is of microphysical origin and confirms that HNO_3 was taken up in PSC particles. For 2000, the low normalized HNO_3 total columns between days 80 and 90 correspond to days when the instrument sampled inside the vortex. The same is true for 2005, days 81 to 82, and 2007, days 68 to 83, but none of these low values is as pronounced as those seen in 2011.

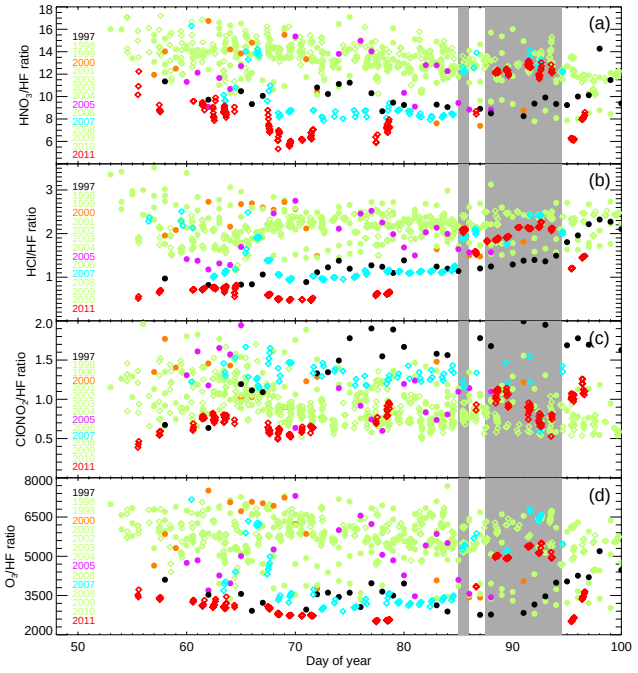

Fig. 6. Spring time series of **(a)** HNO_3, **(b)** HCl, **(c)** $ClONO_2$, and **(d)** ozone, normalized by HF total columns, from 1997 to 2011. Filled circles represent DA8 ratios and open diamonds represent 125HR ratios. The colors correspond to different years as shown in the legend. The gray shading has the same meaning as in Fig. 5.

The 2011 HCl/HF and $ClONO_2$/HF ratios (Fig. 6b and c, respectively), exhibit behavior similar to the total columns shown in Fig. 5b and c. Low values are again seen for days 68–71 (9–12 March), and are evidence of chemical activation on the surfaces of PSC particles. After day 77, the normalized values slowly increase, as the active chlorine returns into the reservoir species HCl and $ClONO_2$. In 1997 and 2007, for measurements within the vortex, the HCl/HF ratios are lower (except for 2011) while the $ClONO_2$/HF ratios are higher than during other years. These show the overshoot of $ClONO_2$ when the active chlorine returns into this reservoir.

The O_3/HF ratio maintains its very low values, being consistently below 4000 for days 55–78 (24 February–19 March), and much lower than most of the normalized ozone values from previous years. These low values are evidence of chemical ozone depletion given the meteorological conditions and all observations presented above. The minimum normalized value is 2489 and occurs on day 77 (18 March), right after the period when we see the chlorine activation. Ozone inside the vortex remains low, the normalized ozone value on day 95 (5 April) when the instrument again sampled vortex air masses, is as low as 2503. The ratios are much higher for the measurements performed outside the vortex, as highlighted by the shaded region. For the other cold years, the normalized ozone values are also low within the vortex, with 1997 and 2007 values being close to those in 2011 for some days, but none of them smaller than those seen in 2011.

To conclude, normalizing with HF reduced the dynamical effects, thus highlighting interannual differences due to chemistry. The low values of normalized HNO_3, HCl, and $ClONO_2$ that occurred on days 68–71, followed by the minimum in normalized ozone that occurred on day 77, are indicative of chlorine activation on cold aerosol particles followed by chemical ozone destruction. Since the 125HR is a sun-dependent instrument, we do not have measurements inside the vortex (late in the fall and during the polar night) from times without chemical loss, and so we are not able to define a baseline for quantifying chemical loss using only measurements. For a quick estimate of the chemical ozone depletion, we can assume a standard O_3/HF ratio of 4500 on the edge and inside the polar vortex (e.g., Mellqvist et al., 2002). Using this value, a column loss of 34 % can be calculated from ((4500–2977)/4500), where 2977 is the mean O_3/HF value for 2011 measurements inside the vortex. Since this approach is oversimplified and has not been validated, a more rigorous method is needed to confirm this result. The methods commonly used to estimate chemical ozone loss are: the ozone/tracer correlation method (Müller et al, 2002; Tilmes et al., 2003), the Match method (Schulz et al., 2000), the vortex-average method (Christensen et al., 2005), the Lagrangian transport calculation method (Manney et al., 2003), and the passive subtraction method (Manney et al, 1995; Goutail et al., 1999; Feng et al., 2005). In this study, the passive subtraction method was used to quantify the chemical ozone depletion above Eureka.

4 Comparisons with a chemical transport model

SLIMCAT (Chipperfield, 2006) is a three-dimensional off-line chemical transport model. It differs from a general circulation model in that the chemistry component is not integrated into the dynamical model, but is off-line and performed separately for each time-step. This model has been used for many studies of ozone and ozone-related gases in the polar regions (e.g., Chipperfield and Jones, 1999; Solomon et al., 2002; Feng et al., 2007; Manney et al., 2009; Feng et al., 2011). The model uses winds and temperatures from meteorological analyses of the European Centre for Medium-Range Weather Forecasts (ECMWF) to specify the atmospheric transport, and calculates the abundances of chemical species in the troposphere and stratosphere.

Figure 7 shows, from top to bottom, the SLIMCAT (blue triangles) and the 125HR (red diamonds) total columns of ozone, HCl, HNO_3, $ClONO_2$, and HF, along with the corresponding percentage differences. SLIMCAT simulations are compared with 125HR measurements for days 55 to 96 (24 February–6 April). Good agreement can be seen for ozone (panel a) except on days 86–93 (27 March–3 April), when the model total columns are slightly larger than the 125HR

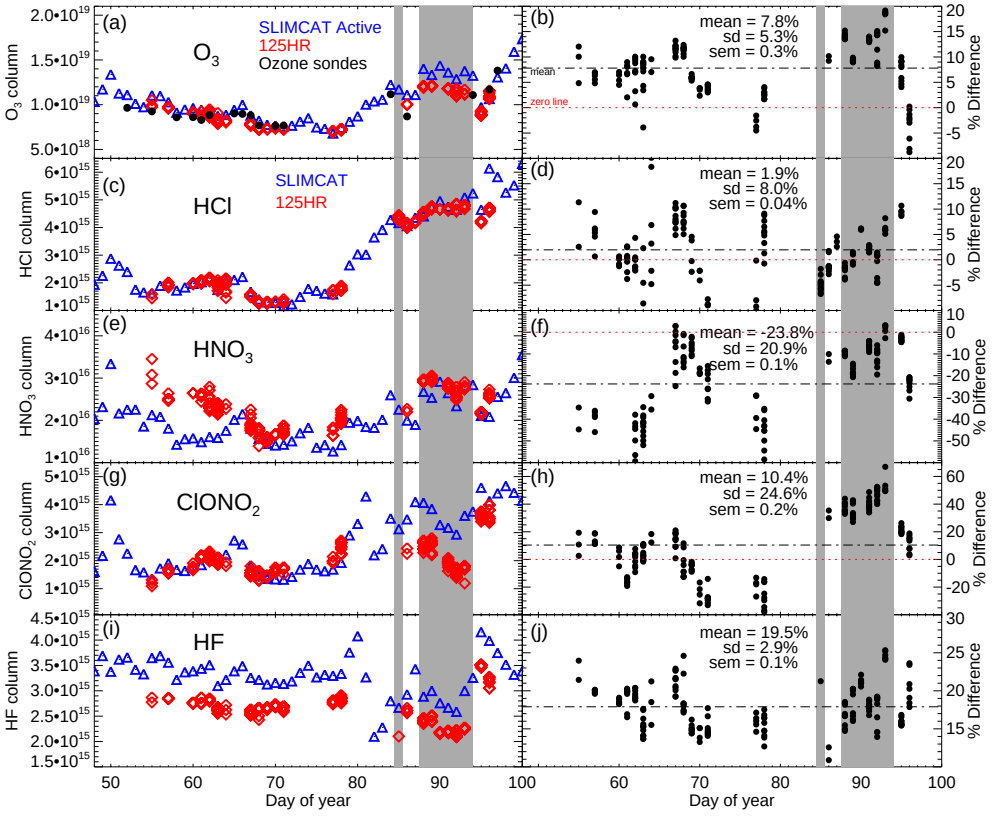

Fig. 7. 125HR (red diamonds) and SLIMCAT (blue triangles) total column comparisons for ozone, HCl, HNO_3, $ClONO_2$, and HF. For ozone, the Eureka ozonesonde measurements (black circles) are also superimposed. In the panels on the left side, the total columns for each gas are shown for the measurements and the model, while in the panels on the right side the corresponding percentage differences are shown. The mean percentage difference, the standard deviation, and the standard error of the mean are also given. These were calculated as described in the text. The gray shading has the same meaning as in Fig. 5.

total columns, likely due to model resolution smoothing over the vortex edge. The mean difference was calculated as

$$\Delta\% = \frac{100}{N}\sum_{i=1}^{N}\left[\left(\mathrm{MODEL}_{\mathrm{TC}}^{(i)} - 125\mathrm{HR}_{\mathrm{TC}}^{(i)}\right)/125\mathrm{HR}_{\mathrm{TC}}^{(i)}\right] \quad (1)$$

where $125\mathrm{HR}_{\mathrm{TC}}^{(i)}$ is the total column measured by the 125HR and $\mathrm{MODEL}_{\mathrm{TC}}^{(i)}$ is the total column simulated by the model, for day i. For ozone, we found a mean percentage difference of 7.8±0.3 %, where the given error is the standard error of the mean. The standard error of the mean relative difference between the model and the 125HR total column (*sem*, in percent) has been evaluated as $sd/\sqrt{N}$, in which *sd* is the statistical 1-sigma (1σ) standard deviation of the observed differences, and N is the number of coincidences. The *sem* provides a measure of the significance of an observed bias (e.g., De Mazière et al., 2008).

For HCl, the agreement between SLIMCAT and the 125HR total columns is good for the entire period, the mean percentage difference being 1.9±0.04 %. The modeled HNO_3 total columns show a negative bias of −23.8±0.1 % compared to the measurements, which is more pronounced at the beginning of the measurement period. This may indicate a limited treatment of the PSCs in the model. For $ClONO_2$, we have good agreement except on days 86–93 (27 March–3 April) as in the case of ozone. For these days, SLIMCAT total columns are larger than those for the 125HR. The mean percentage difference calculated for all the $ClONO_2$ data is 10.4±0.2 %.

The HF total columns for the 125HR and for the model exhibit a similar evolution from days 55 to 96 (24 February to 6 April), but there is a positive bias in the simulated values, SLIMCAT total columns being larger by 19.5±0.1 %. SLIMCAT overestimates the total column abundance of HF in the lowermost stratosphere, the result being a positive bias compared to the measurements. A similar result, 22.54±6.55 % (here $\pm1\sigma$), was found by Duchatelet et al. (2010), when comparing SLIMCAT HF total columns with mid-latitude ground-based FTIR total columns, for the 1984–2009 period.

To quantify chemical ozone loss, we used SLIMCAT and the passive subtraction method. SLIMCAT can be run in two modes: one with full chemistry and dynamics (the "active" run) and one in which ozone is treated as a passive dynamical

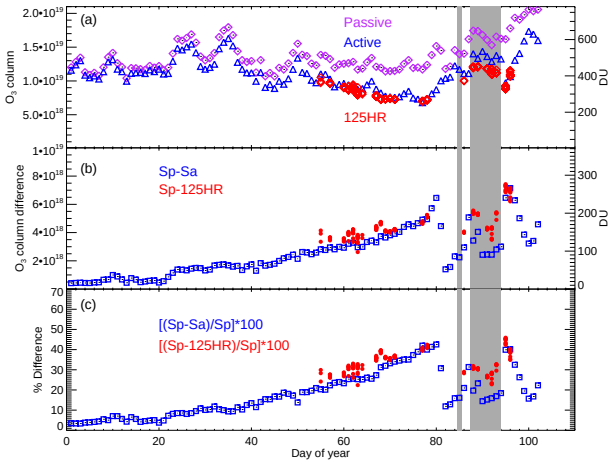

Fig. 8. (a) Passive (purple) and active (blue) SLIMCAT, and the 125HR (red) ozone total columns. **(b)** The absolute differences between the SLIMCAT passive (Sp) and active (Sa) ozone columns (blue squares) and the differences between the SLIMCAT passive (Sp) ozone and the measured (125HR) total columns (red circles). Panel **(c)** is similar to panel **(b)**, but for the percentage differences calculated for the two cases. The gray shading has the same meaning as in Fig. 5.

tracer with no chemistry (the "passive" run). In this method, differences between the measured ozone total columns and those from the passive model runs are assumed to be due to chemistry (Manney et al, 1995; Goutail et al., 1999; Feng et al., 2005).

The SLIMCAT active ozone total columns are shown together with the passive ozone total columns in Fig. 8a. While at the beginning of January there is no significant difference between the two time series, they begin to diverge in mid-January, reaching a maximum difference on day 80 (21 March). The differences vary from day 81 (22 March) to the end of the period, with a second maximum difference on day 95 (5 April). The evolution of the absolute differences between the passive and active SLIMCAT ozone (blue squares) can be seen in Fig. 8b. The maximum difference of 266 DU was reached on day 95 (5 April). The differences between the SLIMCAT passive ozone total columns and the 125HR measured total columns are shown with red circles. These differences are slightly larger than the passive – active SLIMCAT differences. The maximum difference in this case was reached on the same day, day 95, being 276 DU and 3.6 % higher than the model maximum difference.

The corresponding percentage difference between the passive and active SLIMCAT ozone is shown in panel c. To quantify the chemical ozone depletion inside the vortex, we calculated the mean percentage difference, excluding the days when the instrument sampled out of the vortex. The mean percentage difference, which represents the chemical ozone depletion above Eureka from 24 February to 6 April, is then 35 %.

5 Conclusions

As a consequence of dynamically variable meteorological conditions, springtime Arctic ozone levels exhibit significant interannual variability in the lower stratosphere. Meteorological conditions during winter/spring 2011 were particularly favorable to the formation of a strong vortex that lasted into April. Temperatures above Eureka were persistently low, and below the type I PSC threshold in the lower stratosphere for an extended period. PSCs were observed over Eureka by CALIPSO and by the CRL between 11 and 17 February and between 8 and 12 March, respectively.

The spring 2011 ozone, HCl, HNO_3, $ClONO_2$, and HF measurements made at Eureka using the Bruker 125HR FTIR spectrometer are consistent with the occurrence of significant chemical ozone depletion. Unusually low ozone columns were measured from mid-February to late March compared to the previous 14 yr. The normalized O_3/HF, HCl/HF, and HNO_3/HF ratios, for which the effects of dynamics have been reduced, also showed record minima over this period. The normalized HNO_3 columns decreased during the period when temperatures were below the NAT formation threshold. The normalized HCl and $ClONO_2$ columns also decreased during the same period, indicating chlorine activation. The normalized ozone columns showed minima immediately after the chlorine activation period, confirming the occurrence of ozone chemical processing.

The SLIMCAT and 125HR total columns showed good agreement for ozone, HCl, and $ClONO_2$, with larger differences for HNO_3 and HF. SLIMCAT was used to quantify chemical ozone loss using the passive subtraction method. Chemical ozone depletion inside the vortex above Eureka was estimated to be 35 %, consistent with the record ozone loss observed in the Arctic vortex in 2011 (Balis et al., 2011; Manney et al., 2011; Adams et al., 2012).

Supplementary material related to this article is available online at: http://www.atmos-chem-phys.net/12/3821/2012/acp-12-3821-2012-supplement.zip.

Acknowledgements. The authors wish to thank the staff at the Eureka weather station and CANDAC for the logistical and on-site support provided at Eureka. Thanks to CANDAC/PEARL operators Ashley Harrett, Alexei Khmel, Paul Loewen, Keith MacQuarrie, Oleg Mikhailov, and Matt Okraszewski, for their invaluable assistance in maintaining the Bruker 125HR and for taking measurements. CANDAC and PEARL are funded by the Atlantic Innovation Fund/Nova Scotia Research Innovation Trust, Canadian Foundation for Climate and Atmospheric Sciences, Canada Foundation for Innovation, Canadian Space Agency (CSA), Environment Canada (EC), Government of Canada International Polar Year funding, Natural Sciences and Engineering Research Council (NSERC), Ontario Innovation Trust, Polar Continental Shelf Program and the

Ontario Research Fund. The springtime Canadian Arctic ACE Validation Campaigns are supported by the CSA, EC, NSERC, and the Northern Scientific Training Program. Thanks to EC for launching the radiosondes and making the data available.

The authors also wish to thank the Met Office for the stratospheric assimilated data and the British Atmospheric Data Centre for providing access to these data, NASA's Global Modeling and Assimilation Office for the GEOS-5 meteorological data and ECMWF for meteorological analyses used by SLIMCAT.

Work at the Jet Propulsion Laboratory, California Institute of Technology was done under contract with the National Aeronautics and Space Administration.

Edited by: N. Harris

References

Adams, C., Strong, K., Zhao, X., Bassford, M. R., Chipperfield, M. P., Daffer, W., Drummond, J. R., Farahani, E. E., Feng, W., Fraser, A., Goutail, F., Manney, G., McLinden, C. A., Pazmino, A., Rex, M. and Walker, K. A.: Severe 2011 ozone depletion assessed with 11 years of ozone, NO2, and OClO measurements at 80N, Geophys. Res. Lett., 39, L05806, doi:10.1029/2011GL050478, 2012.

Balis, D., Isaksen, I. S. A., Zerefos, C., Zyrichidou, I., Eleftheratos, K., Tourpali, K., Bojkov, R., Rognerud, B., Stordal, F., Sovde, O. A., and Orsolini, Y.: Observed and modeled record ozone decline over the Arctic during winter/spring 2011, Geophys. Res. Lett., 38, L23801, doi:10.1029/2011GL049259, 2011.

Batchelor, R. L., Strong, K., Lindenmaier, R., Mittermeier, R. L., Fast, H., Drummond, J. R., and Fogal, P. F.: A new Bruker IFS 125HR FTIR spectrometer for the Polar Environment Atmospheric Research Laboratory at Eureka, Canada-measurements and comparison with the existing Bomem DA8 spectrometer, J. Atmos. Oceanic Technol., 26, 1328–1340, 2009.

Batchelor, R. L., Kolonjari, F., Lindenmaier, R., Mittermeier, R. L., Daffer, W., Fast, H., Manney, G., Strong, K., and Walker, K. A.: Four Fourier transform spectrometers and the Arctic polar vortex: instrument intercomparison and ACE-FTS validation at Eureka during the IPY springs of 2007 and 2008, Atmos. Meas. Tech., 3, 51–66, doi:10.5194/amt-3-51-2010, 2010.

Bojkov, R. D., Bishop, L., and Fioletov, V. E.: Total ozone trends from quality-controlled ground-based data (1964-1994), J. Geophys. Res., 100, 25867–25876, 1995.

Chipperfield, M. P. and R. L. Jones: Relative influences of atmospheric chemistry and transport on Arctic ozone trends, Nature, 400, 551–554, 1999.

Chipperfield, M. P.: New version of the TOMCAT/SLIMCAT offline chemical transport model: Intercomparison of stratospheric tracer experiments, Q. J. Roy. Meteorol. Soc., 132, 1179–1203, 2006.

Christensen, T., Knudsen, B. M., Streibel, M., Andersen, S. B., Benesova, A., Braathen, G., Claude, H., Davies, J., De Backer, H., Dier, H., Dorokhov, V., Gerding, M., Gil, M., Henchoz, B., Kelder, H., Kivi, R., Kyrö, E., Litynska, Z., Moore, D., Peters, G., Skrivankova, P., St "ubi, R., Turunen, T., Vaughan, G., Viatte, P., Vik, A. F., von der Gathen, P., and Zaitcev, I.: Vortex-averaged Arctic ozone depletion in the winter 2002/2003, Atmos. Chem. Phys., 5, 131–138, doi:10.5194/acp-5-131-2005, 2005.

Chshyolkova, T., Manson, A. H., Meek, C. E., Aso, T., Avery, S. K., Hall, C. M., Hocking, W., Igarashi, K., Jacobi, C., Makarov, N., Mitchell, N., Murayama, Y., Singer, W., Thorsen, D., and Tsutsumi, M.: Polar vortex evolution during Northern Hemispheric winter 2004/05, Ann. Geophys., 25, 1279–1298, doi:10.5194/angeo-25-1279-2007, 2007.

Coy, L., Nash, E. R., and Newman P. A.: Meteorology of the polar vortex: Spring 1997, Geophys. Res. Lett., 24, 2693–2696, 1997.

De Mazière, M., Vigouroux, C., Bernath, P. F., Baron, P., Blumenstock, T., Boone, C., Brogniez, C., Catoire, V., Coffey, M., Duchatelet, P., Griffith, D., Hannigan, J., Kasai, Y., Jones, N., Mahieu, E., Manney, G. L., Piccolo, C., Randall, C., Robert, C., Senten, C., Strong, K., Taylor, J., Tétard, C., Walker, K. A., and Wood, S.: Validation of ACE-FTS v2.2 methane profiles from the upper troposphere to the lower mesosphere, Atmos. Chem. Phys., 9, 2421–2435, doi:10.5194/acp-9-2421-2008, 2008.

Donovan, D. P., Fast, H., Makino, Y., Bird, J. C., Carswell, A. I., Davies, J., Duck, T. J., Kaminski, J. W., McElroy, C. T., Mittermeier, R. L., Pal, S. R., Savastiouk, V., Velkov, D., and Whiteway, J. A.: Ozone, column ClO, and PSC measurements made at the NDSC Eureka observatory (80° N, 86° W) during the spring of 1997, Geophys. Res. Lett., 24, 2709–2712, 1997.

Drdla, K. and Schoeberl, M. R.: Microphysical modeling of the 1999–2000 Arctic winter: 2. Chlorine activation and ozone depletion, J. Geophys. Res., 108, 8319, 15 pp.,doi:10.1029/2001JD001159, 2003.

Duchatelet, P., Demoulin, P., Hase, F., Ruhnke, R., Feng, W., Chipperfield, M. P., Bernath, P. F., Boone, C. D., Walker, K. A., and Mahieu, E.: Hydrogen fluoride total and partial column time series above the Jungfraujoch from long-term FTIR measurements: Impact of the line-shape model, characterization of the error budget and seasonal cycle, and comparison with satellite and model data, J. Geophys. Res., 115, D22306, doi:10.1029/2010JD014677, 2010.

Fairlie, T. D. A.: Three-dimensional transport simulations of the dispersal of volcanic aerosol from Mount Pinatubo, Q. J. Roy. Meteorol. Soc., 121, 1943–1980, doi:10.1256/smsqj.52808, 1995.

Farahani, E. E., Fast, H., Mittermeier, R. L., Makino, Y., Strong, K., McLandress, C., Shepherd, T. G., Chipperfield, M. P., Hannigan, J. W., Coffey, M. T., Mikuteit, S., Hase, F., Blumenstock, T., and Raffalski, U.: Nitric acid measurements at Eureka obtained in winter 2001-2002 using solar and lunar Fourier transform absorption spectroscopy: comparisons with observations at Thule and Kiruna and with results from three-dimensional models, J. Geophys. Res., 112, D01305, doi:10.1029/2006JD007096, 2007.

Farman, J. C., Gardiner, B. G., and Shanklin, J. D.: Large losses of total ozone in Antarctica reveal seasonal ClO_x/NO_x interaction, Nature, 315, 207–210, 1985.

Fast, H., Mittermeier, R. L., and Makino Y.: A ten-year record of Arctic trace gas total column measurements at Eureka, Canada, from 1997 to 2006, Atmos.-Ocean, 49, 67–94, 2011.

Feng, W., Chipperfield, M. P., Davies, S., Sen, B., Toon, G., Blavier, J. -F., Webster, C. R., Volk, C. M., Ulanovsky, A., Ravegnani, F., von der Gathen, P., Jost, H., Richard, E. C., and Claude, H.: Three-dimensional model study of the Arctic ozone loss in 2002/2003 and comparison with 1999/2000 and 2003/2004, Atmos. Chem. Phys., 5, 139–152, doi:10.5194/acp-5-139-2005,

2005.

Feng, W., Chipperfield, M. P., Davies, S., von der Gathen, P., Kirö, E., Volk, C. M., Ulanovsky, A., and Belyaev, G.: Large chemical ozone loss in 2004/2005 Arctic winter/spring, Geophys. Res. Lett., 34, L09803, doi:10.1029/2006GL029098, 2007.

Feng, W., Chipperfield, M. P., Davies, S., Mann, G. W., Carslaw, K. S., Dhomse, S., Harvey, L., Randall, C., and Santee, M. L.: Modelling the effect of denitrification on polar ozone depletion for Arctic winter 2004/2005, Atmos. Chem. Phys., 11, 6559–6573, doi:10.5194/acp-11-6559-2011, 2011.

Fioletov, V. E., Kerr, J. B., Wardle, D. I., Davies, J., Hare, E. W., McElroy, C. T., and Tarasick, D. W.: Long-term ozone decline over the Canadian Arctic to early 1997 from ground-based and balloon observations, Geophys. Res. Lett., 24, 2705–2708, 1997.

Fu, D., Walker, K. A., Mittermeier, R. L., Strong, K., Sung, K., Fast, H., Bernath, P. F., Boone, C. D., Daffer, W. H., Fogal, P., Kolonjari, F., Loewen, P., Manney, G. L., Mikhailov O., and Drummond J. R.: Simultaneous trace gas measurements using two Fourier transform spectrometers at Eureka, Canada during spring 2006, and comparisons with the ACE–FTS, Atmos. Chem. Phys., 11, 5383–5405, doi:10.5194/acp-11-5383-2011, 2011.

Goutail, F., Pommereau, J.-P., Phillips, C., Daniel, C., Sarkissian, A., Lefèvre, F., Kyrö, E., Rummukainen, M., Ericksen, P., Andersen, S. B., Kaastad-Hoiskar, B.-A., Braathen, G., Dorokhov, V., and Khattatov, V. U.: Depletion of column ozone in the Arctic during the winters 1993–94 and 1994–95, J. Atmos. Chem., 32, 1–34, 1999.

Goutail, F., Pommereau, J.-P., Lefèvre, F., van Roozendael, M., Andersen, S. B., Kaastad-Hoiskar, B.-A., Dorokhov, V., Kyrö, E., Chipperfield, M. P., and Feng, W.: Early unusual ozone loss during the Arctic winter 2002/2003 compared to other winters, Atmos. Chem. Phys, 5, 665–677, doi:10.5194/acp-5-665-2005, 2005.

Harvey, V. L., Pierce, R. B., Fairlie, T. D., and Hitchman, M. H.: A climatology of stratospheric polar vortices and anticyclones, J. Geophys. Res., 107, 4442, doi:10.1029/2001JD001471, 2002.

Hofmann, D. J. and Oltmans, S. J.: Anomalous Antarctic ozone during 1992: Evidence for Pinatubo volcanic aerosol effects, J. Geophys. Res., 98, 18555–18562, 1993.

Jin, J. J., Semeniuk, K., Manney, G. L., Jonsson, A. I., Beagley, S. R., McConnell, J. C., Dufour, G., Nassar, R., Boone, C. D., Walker, K. A., Bernath, P. F., and Rinsland, C. P.: Severe Arctic ozone loss in the winter 2004/2005: observations from ACE-FTS, Geophys. Res. Lett., 33, L15801, doi:10.1029/2006GL026752, 2006.

Kohlhepp, R., Ruhnke, R., Chipperfield, M. P., De Mazière, M., Notholt, J., Barthlott, S., Batchelor, R. L., Blatherwick, R. D., Blumenstock, Th., Coffey, M. T., Demoulin, P., Fast, H., Feng, W., Goldman, A., Griffith, D. W. T., Hamann, K., Hannigan, J. W., Hase, F., Jones, N. B., Kagawa, A., Kaiser, I., Kasai, Y., Kirner, O., Kouker, W., Lindenmaier, R., Mahieu, E., Mittermeier, R. L., Monge-Sanz, B., Morino, I., Murata, I., Nakajima, H., Palm, M., Paton-Walsh, C., Raffalski, U., Reddmann, Th., Rettinger, M., Rinsland, C. P., Rozanov, E., Schneider, M., Senten, C., Servais, C., Sinnhuber, B.-M., Smale, D., Strong, K., Sussmann, R., Taylor, J. R., Vanhaelewyn, G., Warneke, T., Whaley, C., Wiehle, M., and Wood, S. W.: Observed and simulated time evolution of HCl, $ClONO_2$, and HF total column abundances, Atmos. Chem. Phys., 12, 3527–3556, doi:10.5194/acp-12-3527-2012, 2012.

Labitzke, K. and collaborators: The Berlin stratospheric data series CD from Meteorological Institute, Freie Universität Berlin, Germany, 2002.

Langematz, U. and Kunze, M.: An update on dynamical changes in the Arctic and Antarctic stratospheric polar vortices, Clim. Dynam., 27, 647–660, 2006.

Lowe, D. and MacKenzie, A. R.: Polar stratospheric cloud microphysics and chemistry, J. Atmos. Solar-Terr. Phys., 70, 13–40, 2008.

Mankin, W. G., Coffey, M. T., Goldman, A., Schoeberl, M. R., Lait, L. R., and Newman, P. A.: Airborne measurements of stratospheric constituents over the Arctic in the winter of 1989, Geophys. Res. Lett., 17, 473–476, 1990.

Manney, G. L., Zurek, R. W., O'Neill, A., and Swinbank, R.: On the motion of air through the stratospheric polar vortex, J. Atmos. Sci., 51, 2973–2994, 1994.

Manney, G. L., Zurek, R. W., Froidevaux, L., Waters, J. W., O'Neill, A., and Swinbank, R.: Lagrangian transport calculations using UARS data. Part II – Ozone, J. Atmos. Sci., 52, 3069–3081, 1995.

Manney, G. L., Froidevaux, L., Santee, M. L., Zurek, R. W., and Waters, J. W.: MLS observations of Arctic ozone loss in 1996-97, Geophys. Res. Lett., 24, 2697–2700, 1997.

Manney, G. L., Froidevaux, L., Santee, M. L., Livesey, N. J., Sabutis, J. L., and Waters, J. W.: Variability of ozone loss during Arctic winter (1999–2000) estimated from UARS Microwave Limb Sounder measurements, J. Geophys. Res., 108, 4149, 15 pp., doi:10.1029/2002JD002634, 2003.

Manney, G. L., Santee, M. L., Froidevaux, L., Hoppel, K., Livesey, N. J., and Waters, J. W.: EOS MLS observations of ozone loss in the 2004–2005 Arctic winter, Geophys. Res. Lett., 33, L04802, doi:10.1029/2005GL024494, 2006.

Manney, G. L., Daffer, W. H., Zawodny, J. M., Bernath, P. F., Hoppel, K. W., Walker, K. A., Knosp, B. W., Boone, C., Remsberg, E. E., Santee, M. L., Harvey, V. L., Pawson, S., Jackson, D. R., Deaver, L., McElroy, C. T., McLinden, C. A., Drummond, J. R., Pumphrey, H. C., Lambert, A., Schwartz, M. J., Froidevaux, L., McLeod, S., Takacs, L. L., Suarez, M. J., Trepte, C. R., Cuddy, D. C., Livesey, N. J., Harwood, R. S., and Waters, J. W.: Solar occultation satellite data and derived meteorological products: Sampling issues and comparisons with Aura Microwave Limb Sounder, J. Geophys. Res., 112, D24550, doi:10.1029/2007JD008709, 2007.

Manney, G. L., Harwood, R. S., MacKenzie, I. A., Minschwaner, K., Allen, D. R., Santee, M. L., Walker, K. A., Hegglin, M. I., Lambert, A., Pumphrey, H. C., Bernath, P. F., Boone, C. D., Schwartz, M. J., Livesey, N. J., Daffer, W. H., and Fuller, R. A.: Satellite observations and modeling of transport in the upper troposphere through the lower mesosphere during the 2006 major stratospheric sudden warming, Atmos. Chem. Phys., 9, 4775–4795, doi:10.5194/acp-9-4775-2009, 2009.

Manney, G. L., Santee, M. L., Rex, M., Livesey, N. J., Pitts, M. C., Veefkind, P., Nash, E. R., Wohltmann, I., Lehmann, R., Froidevaux, L., Poole, L. R., Schoeberl, M. R., Haffner, D. P., Davies, J., Dorokhov, V., Gernandt, H., Johnson, B., Kivi, R., Kyrö, E., Larsen, N., Levelt, P. F., Makshtas, A., McElroy, C. T., Nakajima, H., Parrondo, M. C., Tarasick, D. W., von der Gathen, P., Walker, K. A., and N. S. Zinoviev (2011), Unprecedented Arctic Ozone

Loss in 2011, Nature, 478, 469–475, doi:10.1038/nature10556, 2011.

Manson, A. H., Meek, C. E., and Chshyolkova, T.: Regional Stratospheric Warmings in the Pacific-Western Canada (PWC) Sector during Winter 2004/5: Implications for Temperatures, Winds, Chemical Constituents and the Characterization of the Polar Vortex, Ann. Geophys., 26, 3597–3622, doi:10.5194/angeo-26-3597-2009, 2008.

McPeters, R. D., Hollandsworth, S. M., Flynn, L. E., Herman, J. R., and Seftor, C. J.: Long-term ozone trends derived from the 16-year combined Nimbus 7/Meteor 3 TOMS Version 7 record, Geophys. Res. Lett., 23, 3699–3702, 1996.

Mellqvist, J., Galle, B., Blumenstock, T., Hase, F., Yashcov, D., Notholt, J., Sen, B., Blavier, J.-F., Toon, G. C., and Chipperfield, M. P.: Ground-based FTIR observations of chlorine activation and ozone depletion inside the Arctic vortex during the winter of 1999/2000, J. Geophys. Res., 107, 8263, 16 pp., doi:10.1029/2001JD001080, 2002.

Müller, R., Tilmes, S., Grooß, J.-U., McKenna, D. S., Müller, M., Schmidt, U., Toon, G. C., Stachnik, R. A., Margitan, J. J., Elkins, J. W., Arvelius, J., and Russell III, J. M.: Chlorine activation and chemical ozone loss deduced from HALOE and balloon measurements in the Arctic during the winter of 1999–2000, J. Geophys. Res., 108 (D5), doi:10.1029/2001JD001423, 2003.

Nash, E. R., Newman, P. A., Rosenfield, J. E., and Schoeberl, M. R.: An objective determination of the polar vortex using Ertel's potential vorticity, J. Geophys. Res., 101, 9471–9478, 1996.

Newman, P. A., Gleason, J. F., McPeters, R. D., and Stolarski, R. S.: Anomalously low ozone over the Arctic, Geophys. Res. Lett., 24, 2689–2692, 1997.

Nott, G. J., Duck, T. J., Doyle, J. G., Coffin, M. E. W., Perro, C., Thackray, C. P., Drummond, J. R., Fogal, P. F., McCullough, E., and Sica, R. J.: A remotely-operated lidar for aerosol, temperature, and water vapor profiling in the High Arctic, J. Atmos. Ocean. Technol., 29, 221–234, 2012.

Orsolini, Y. J., Stephenson, D. B., and Doblas-Reyes, F. J.: Storm track signature in total ozone during Northern Hemisphere winter, Geophys. Res. Lett., 25, 2413–2416, doi:10.1029/98GL01852, 1998.

Paton-Walsh, C., Mittermeier, R. L., Bell, W., Fast, H., Jones, N., and Meier, A.: An intercomparison of ground-based solar FTIR measurements of atmospheric gases at Eureka, Canada, J. Atmos. Oceanic Technol., 25, 2028–2036, 2008.

Pawson, S., Labitzke, K., Leder, S.: Stepwise changes in stratospheric temperature, Geophys. Res. Lett., 25, 2157–2160, 1998.

Pawson, S. and Naujokat, B.: The cold winters of the middle 1990s in the northern lower stratosphere, J. Geophys. Res., 104, 14209–14222, 1999.

Petzoldt, K.: The role of dynamics in total ozone deviations from their long-term mean over the Northern Hemisphere, Ann. Geophys., 17, 231–241, 1999, http://www.ann-geophys.net/17/231/1999/.

Pitts, M. C., Poole, L. R., and Thomason, L. W.: CALIPSO polar stratospheric cloud observations: second-generation detection algorithm and composition discrimination, Atmos. Chem. Phys., 9, 7577–7589, doi:10.5194/acp-9-7577-2009, 2009.

Poole, L. R., McCormick, M. P.: Airborne lidar observations of arctic polar stratospheric clouds: indications of two distinct growth stages. Geophys. Res. Lett., 15, 21–23, 1988.

Portmann, R. W., Solomon, S., Garcia, R. R., Thomason, L. W., Poole, L. R., and McCormick, M. P.: Role of aerosol variations in anthropogenic ozone depletion in the polar regions, J. Geophys. Res., 101, 22991–23006, 1996.

Pougatchev, N. S., Connor, B. J., and Rinsland, C. P.: Infrared measurements of the ozone vertical distribution above Kitt Peak, J. Geophys. Res., 100, 16689–16697, 1995.

Rex, M., Salawitch, R. J., von der Gathen, P., Harris, N. R. P., Chipperfield, M. P., and Naujokat, B.: Arctic ozone loss and climate change, Geophys. Res. Lett., 31, L04116, doi:10.1029/2003GL018844, 2004.

Rex, M., Salawitch, R. J., Deckelmann, H., von der Gathen, P., Harris, N. R. P., Chipperfield, M. P., Naujokat, B., Reimer, E., Allaart, M., Andersen, S. B., Bevilacqua, R., Braathen, G. O., Claude, H., Davies, J., De Backer, H., Dier, H., Dorokhov, V., Fast, H., Gerding, M., Godin-Beekmann, S., Hoppel, K., Johnson, B., Kyrö, E., Litynska, Z., Moore, D., Nakane, H., Parrondo, M. C., Risley Jr., A. D., Skrivankova, P., Stübi, R., Viatte, P., Yushkov, V., and Zerefos, C.: Arctic winter 2005: Implications for stratospheric ozone loss and climate change, Geophys. Res. Lett., 33, L23808, doi:10.1029/2006GL026731, 2006.

Rienecker, M. M., Suarez, M. J., Todling, R., Bacmeister, J., Takacs, L., Liu, H.-C., Gu, W., Sienkiewicz, M., Koster, R. D., Gelaro, R., Stajner, I., and Nielsen, J. E.: The GEOS-5 data assimilation system - Documentation of versions 5.0.1, 5.1.0, and 5.2.0, NASA Tech. Memo., TM-2008-104606, 27, 2008.

Rienecker, M. M., Suarez, M. J., Gelaro, R., Todling, R., Bacmeister, J., Liu, E. et al.: MERRA – NASA's Modern-Era Retrospective Analysis for Research and Applications, J. Clim., 24, 3624–3648, 2011.

Rinsland, C. P., Smith, M. A. H., Rinsland, P. L., Goldman, A., Brault, J. W., and Stokes, G. M.: Ground-based infrared spectroscopic measurements of atmospheric hydrogen cyanide, J. Geophys. Res., 87, 11119–11125, 1982.

Rinsland, C. P., Goldman, A., Murcray, F. J., Murcray, F. H., Blatherwick, R. D., and Murcray, D. G.: Infrared measurements of atmospheric gases above Mauna Loa, Hawaii, in February 1987, J. Geophys. Res., 91, 12607–12626, 1988.

Rodgers, C. D.: Retrieval of atmospheric temperature and composition from remote measurements of thermal radiation. Rev. Geophys., 14, 609–624, 1976.

Rodgers, C. D.: Characterization and error analysis of profiles retrieved from remote sounding measurements, J. Geophys. Res., 95, 5587–5595, 1990.

Rodgers, C. D.: Inverse Methods for Atmospheric Sounding: Theory and Practice, World Scientific Publishing Co. Pte. Ltd., 238, 2000.

Rodgers, C. D. and Connor, B. J.: Intercomparison of remote sounding instruments, J. Geophys. Res., 108, 4116, doi:10.1029/2002JD002299, 2003.

Rösevall, J. D., Murtagh, D. P., and Urban, J.: Ozone depletion in the 2006/2007 Arctic winter, Geophys. Res. Lett., 34, L21809, doi:10.1029/2007GL030620, 2007.

Rösevall, J. D., Murtagh, D. P., Urban, J., Feng, W., Eriksson, P., and Brohede, S.: A study of ozone depletion in the 2004/2005 Arctic winter based on data from Odin/SMR and Aura/MLS, J. Geophys. Res., 113, D13301, doi:10.1029/2007JD009560, 2008.

Rothman, L. S.,R. R. Gamache, R. H. Tipping, C. P. Rinsland, M. A. H. Smith, D. C. Benner, V. Malathy Devi, J.-M. Flaud, C. Camy-

Peyret, A. Perrin, A. Goldman, S. T. Massie, L. R. Brown, and R. A. Toth: The HITRAN molecular database: Editions of 1991 and 1992, J. Quant. Spectrosc. Ra., 48, 469–507, 1992.

Rothman, L. S., Jacquemart, D., Barbe, A., Chris Benner, D., Birk, M., Brown, L. R., Carleer, M. R., Chackerian Jr., C., Chance, K., Coudert, L. H., Dana, V., Devi, V. M., Flaud, J.-M., Gamache, R. R., Goldman, A., Hartmann, J.-M., Jucks, K. W., Maki, A. G., Mandin, J.-Y., Massie, S. T., Orphal, J., Perrin, A., Rinsland, C. P., Smith, M. A. H., Tennyson, J., Tolchenov, R. N., Toth, R. A., Vander Auwera, J., Varanasi, P., and Wagner, G.: The HITRAN 2004 molecular spectroscopic database, J. Quant. Spectrosc. Ra., 96, 139–204, 2005.

Santee, M. L., MacKenzie, I. A., Manney, G. L., Chipperfield, M. P., Bernath, P. F., Walker, K. A., Boone, C. D., Froidevaux, L., Livesey, N. J., and Waters, J. W.: A study of stratospheric chlorine partitioning based on new satellite measurements and modeling, J. Geophys. Res., 113, D12307, doi:10.1029/2007JD009057, 2008.

Schulz, A., Rex, M., Steger, J., Harris, N. R. P., Braathen, G. O., Reimer, E., Alfier, R., Beck, A., Alpers, M., Cisneros, J., Claude, H., De Backer, H., Dier, H., Dorokhov, V., Fast, H., Godin, S., Hansen, G., Kanzawa, H., Kois, B., Kondo, Y., Kosmidis, E., Kyrö, E., Litynska, Z., Molyneux, M. J., Murphy, G., Nakane, H., Parrondo, C., Ravegnani, F., Varotsos, C., Vialle, C., Viatte, P., Yushkov, V., Zerefos, C., von der Gathen, P.: Match observations in the Arctic winter 1996/97: High stratospheric ozone loss rates correlated with low temperatures deep inside the polar vortex, Geophys. Res. Lett., 27, 205–208, doi:10.1029/1999GL010811, 2000.

Singleton, C. S., Randall, C. E., Harvey, V. L., Chipperfield, M. P., Feng, W., Manney, G. L., Froidevaux, L., Boone, C. D., Bernath, P. F., Walker, K. A., McElroy, C. T., and Hoppel, K. W.: Quantifying Arctic ozone loss during the 2004-2005 winter using satellite observations and a chemical transport model, J. Geophys. Res., 112, D07304, doi:10.1029/2006JD007463, 2007.

Solomon, S., Garcia, R. R., Rowland, F. S., and Wuebbles, D. J.: On the depletion of Antarctic ozone, Nature, 321, 755–758, 1986.

Solomon, P., Connor, B., Barrett, J., Mooney, T., Lee, A., and Parrish, A.: Measurements of stratospheric ClO over Antarctica in 1996–2000 and implications for ClO dimer chemistry, Geophys. Res. Lett., 29, 1708, 4 pp., doi:10.1029/2002GL015232, 2002.

SPARC CCMVal, 2010: SPARC report on the evaluation of chemistry-climate models, edited by: Eyring, V., Shepherd, T. G., and Waugh, D. W., SPARC Rep. 5, WCRP-132, WMO/TD-1526.

Steele, H. M., Hamill, P., McCormick, M. P., and Swissler, T. J.: The formation of polar stratospheric clouds, J. Atmos. Sci., 40, 2055–2067, 1983.

Steinbrecht, W., Claude, H., Schönenborn, F., Leiterer, U., Dier, H., Lanzinger, E.: Pressure and temperature differences between Vaisala RS80 and RS92 radiosonde systems, J. Atmos. Ocean. Technol., 25, 909–927, 2008.

Swinbank, R. and O'Neill, A.: A stratosphere-troposphere data assimilation system, Mon. Weather Rev., 122, 688–702, 1994.

Tegtmeier, S., Rex, M., Wohltmann, I., and Krüger, K.: Relative importance of dynamical and chemical contributions to Arctic wintertime ozone, Geophys. Res. Lett., 35, L17801, doi:10.1029/2008GL034250, 2008.

Tilmes, S., Müller, R., Grooß, J.-U., McKenna, D. S., Russell III, J. M., and Sasano, Y.: Calculation of chemical ozone loss in the Arctic winter 1996–1997 using ozone-tracer correlations: Comparison of Improved Limb Atmospheric Spectrometer (ILAS) and Halogen Occultation Experiment (HALOE) results, J. Geophys. Res., 108, 4045, 15 pp., doi:10.1029/2002JD002213, 2003.

Toon, G. C., Farmer, C. B., Schaper, P. W., Lowes, L. L., Norton, R. H., Schoeberl, M. R., Lait, L. R., and Newman, P. A.: Evidence for subsidence in the 1989 Arctic winter stratosphere from airborne infrared composition measurements, J. Geophys. Res., 97, 7963–7970, 1992.

Toon, G. C., Blavier, J.-F., Sen, B., Salawitch, R. J., Osterman, G. B., Notholt, J., Rex, M., McElroy, C. T., and Russell III, J. M.: Ground based observations of Arctic O_3 loss during spring and summer 1997, J. Geophys. Res., 104, 26497–26510, 1999.

Toon, O. B., Tabazadeh, A., and Browell, E. V.: Analysis of lidar observations of Arctic polar stratospheric clouds during January 1989, J. Geophys. Res., 105, 20589–20615, 2000.

Turco, R. P., Toon, O. B., and Hamill, P.: Heterogeneous physiochemistry of the polar ozone hole, J. Geophys. Res., 94, 16493–16510, 1989.

Vigouroux, C., De Mazière, M., Demoulin, P., Servais, C., Hase, F., Blumenstock, T., Kramer, I., Schneider, M., Mellqvist, J., Strandberg, A., Velazco, V., Notholt, J., Sussmann, R., Stremme, W., Rockmann, A., Gardiner, T., Coleman, M., and Woods, P.: Evaluation of tropospheric and stratospheric ozone trends over Western Europe from ground-based FTIR network observations, Atmos. Chem. Phys., 8, 6865–6886, doi:10.5194/acp-8-6865-2008, 2008.

Voigt, C., Schreiner, J., Kohlmann, A., Zink, P., Mauersberger, K., Larsen, N., Deshler, T., Kröger, C., Rosen, J., Adriani, A., Cairo, F., Donfrancesco, G. D., Viterbini, M., Ovarlez, J., Ovarlez, H., David, C., and Dörnbrack, A.: Nitric acid trihydrate (NAT) in polar stratospheric clouds, Science, 290, 1756–1758, 2000.

Vömel, H., Selkirk, H., Miloshevich, L., Valverde-Canossa, J., Valdés, J., Kyrö, E., Kivi, R., Stolz, W., Peng, G., and Diaz, J. A.: Radiation dry bias of the Vaisala RS92 humidity sensor, J. Atmos. Oceanic Technol., 24, 953–963, 2007.

WMO (World Meteorological Organization): Scientific Assessment of Ozone Depletion: 2006, WMO Global Ozone Research and Monitoring Project-Report 50, Geneva, Switzerland, 2007.

WMO (World Meteorological Organization): Scientific Assessment of Ozone Depletion: 2010, WMO Global Ozone Research and Monitoring Project-Report 52, Geneva, Switzerland, 2011.

Xu, X., Manson, A. H., Meek, C. E., Chshyolkova, T., Drummond, J. R., Hall, C. M., Riggin, D. M., and Hibbins, R. E.: Vertical and inter-hemispheric links in the stratosphere-mesosphere as revealed by the day-to-day variability of Aura-MLS temperature data, Ann. Geophys., 27, 3387–3409, 2009, http://www.ann-geophys.net/27/3387/2009/.